Astronomy & Astrophysics manuscript no. output
September 26, 2025

Dynamical mass of a solar-like oscillator at the main-sequence turnoff from *Gaia* astrometry & ground-based spectroscopy

P. G. Beck[1,2], T. Masseron[1,2], K. Pavlovski[3], D. Godoy-Rivera[1,2], S. Mathur[1,2], D. H. Grossmann[1,2], D. B. Palakkatharappil[4], E. Panetier[4], R. A. García[4], J. Merc[5,1], Y. Lu[7], I. Amestoy[8], and H. J. Deeg[1,2]

[1] Instituto de Astrofísica de Canarias, E-38205 La Laguna, Tenerife, Spain e-mail: paul.beck@iac.es
[2] Departamento de Astrofísica, Universidad de La Laguna, E-38206 La Laguna, Tenerife, Spain
[3] Department of Physics, Faculty of Science, University of Zagreb, Zagreb, Croatia
[4] Université Paris-Saclay, Université Paris Cité, CEA, CNRS, AIM, 91191, Gif-sur-Yvette, France
[5] Astronomical Institute, Faculty of Mathematics and Physics, Charles University, V Holešovičkách 2, 180 00 Prague, Czechia
[6] Department of Astronomy, University of Geneva, Chemin Pegasi 51, CH-1290 Versoix, Switzerland
[7] Astrophysics Group, School of Physics and Astronomy, University of Exeter, Stocker Road, Exeter EX4 4QL, UK
[8] IRAP, Université de Toulouse, CNRS, CNES, UPS, 14 avenue Edouard Belin, 31400 Toulouse, France

Submitted: September 27, 2025

ABSTRACT

Asteroseismic scaling relations are widely used for solar-like oscillators, but have lacked dynamical validation on the main sequence due to the absence of eclipsing binaries. We present KIC 9693187 as the first double-lined binary system (SB2) hosting a solar-like oscillating post-main-sequence star whose dynamical masses are derived using *Gaia* astrometry and spectroscopy with the Las Cumbres Observatory network (LCO). By combining *Gaia* DR3 orbital astrometry with LCO spectroscopic monitoring to derive full orbital solutions and masses for non-eclipsing SB2 system, we find $M_1^{\rm dyn} = 0.99 \pm 0.05 M_\odot$ and $M_2^{\rm dyn} = 0.89 \pm 0.04 M_\odot$ for the primary and secondary, respectively. Asteroseismic parameters were extracted from photometry of the NASA *Kepler* satellite. From scaling relations we obtain a mass of $M_1^{\rm SR} = 0.98 \pm 0.18 M_\odot$, which agrees excellently with the dynamical mass. The mass from individual frequency modeling is $M_1^{\rm IF} = 0.92 \pm 0.01 M_\odot$. Taking into account the systematic uncertainty of $0.04\,M_\odot$ for best fit models from individual frequency fitting, we find an agreement within 1.2σ. This approach provides the first empirical validation for main-sequence solar-like oscillators and opens a new window for validating asteroseismology without relying on eclipses, with implications for stellar and galactic studies in the era of ESA's PLATO space mission.

Key words. Asteroseismology – (Stars:) binaries: spectroscopic – Stars: late-type – stars: individual: KIC 9693187.

1. Introduction

Asteroseismic scaling relations, as formulated by Brown et al. (1991), Kjeldsen & Bedding (1995) and Kallinger et al. (2010),

$$\frac{R}{R_\odot} = \left(\frac{\nu_{\rm max}}{\nu_{\rm max}^\odot}\right) \cdot \left(\frac{\Delta\nu}{\Delta\nu_\odot}\right)^{-2} \cdot \left(\frac{T_{\rm eff}}{T_{\rm eff}^\odot}\right)^{1/2}, \quad (1)$$

$$\frac{M}{M_\odot} = \left(\frac{\nu_{\rm max}}{\nu_{\rm max}^\odot}\right)^{3} \cdot \left(\frac{\Delta\nu}{\Delta\nu_\odot}\right)^{-4} \cdot \left(\frac{T_{\rm eff}}{T_{\rm eff}^\odot}\right)^{3/2} = \left(\frac{R}{R_\odot}\right)^{3} \cdot \left(\frac{\Delta\nu}{\Delta\nu_\odot}\right)^{2}, \quad (2)$$

provide a powerful tool to estimate the mass, M and radius, R for solar-like oscillators. These equations use the frequency of oscillatory power excess ($\nu_{\rm max}$), large-frequency separation ($\Delta\nu$) between modes of identical spherical degree (ℓ), and consecutive radial orders (n), and effective temperature ($T_{\rm eff}$) measured from the star and the Sun ($\odot$) as input for these homological relations.

The exquisite photometric quality of space telescopes such as the NASA *Kepler* (Borucki et al. 2010), its refurbished K2 (Howell et al. 2014) or TESS (Transiting Exoplanet Survey Satellite, Ricker et al. 2014) missions have provided rich datasets of solar-like oscillating stars (e.g. García & Ballot 2019). These relations, therefore, are widely applied for large sample studies in galactic archaeology and stellar evolution (e.g. Casagrande et al. 2016; Mathur et al. 2016; Zinn et al. 2022; Bellinger 2020; Pinsonneault et al. 2025), and exoplanet host characterization (e.g. Huber et al. 2022). Despite their broad usage, scaling relations remain semi-empirical and require careful validation across stellar evolutionary phases of solar-like stars.

Scaling relations can be validated in various ways. Eclipsing, double-lined (SB2) binary systems provide model-independent measurements of the stellar masses, constrained from the orbital motion (e.g. Prša 2018). Comparisons of the dynamical with the seismically inferred mass have suggested that asteroseismology could overestimate the stellar mass by up to 15% (Gaulme et al. 2016a; Benbakoura et al. 2021). However, with a total benchmark that amounts to 15 objects, the sample of eclipsing SB2 systems, hosting solar-like oscillators, is scarce, even from the large target ensembles from modern space photometry, and strongly biased to the H-shell burning red-giant branch stars (Beck et al. 2024). While ~30% of all main-sequence (MS) solar-like oscillators are in binary systems (Beck 2025), only few binary components have been seismically studied (White et al. 2017; Metcalfe et al. 2012; Beck et al. 2017; García et al. 2025).

So far, the only direct test for Eq. 2 on the MS was performed by Gaulme et al. (2016b), by studying the actual oscillation of the Sun, by using their reflection on Neptune from K2 photometry. The authors found an overestimated solar mass (~14%) and radius (~4.3%) from the scaling relations; however, they attributed this to the shifted frequencies from enhanced solar activity. Indeed, the best-fit model constrained through individual fre-

quencies led to a mass and radius consistent with simultaneous observations from the ESA Solar and Heliospheric Observatory (SOHO, Domingo et al. 1995). The lack of benchmark systems has left a critical gap in validating asteroseismic scaling relations precisely where they are most often assumed to be robust.

The key challenge in the MS mass regime ($0.8 \lesssim M/M_{\odot} \lesssim 1.6$, K5-F5) has been the lack of systems with known orbital inclinations, which are necessary to derive dynamical masses. Eclipses naturally provide this constraint from their light curve models. However, the third data release (DR3; Gaia Collaboration et al. 2023) from ESA's *Gaia* mission (Gaia Collab. et al. 2016) has opened a new avenue. For a subset of systems, the *Gaia* non-single star catalog (NSS, Gaia Collab. et al. 2023) provides orbital inclinations for astrometric and single-lined binaries (ASB1). While the inclination is normally the bottleneck for the determination of dynamical masses, for the case of astrometric systems this parameter is known. Thus, the missing piece becomes the detection of the spectroscopic signature of the secondary component from ground-based observations.

In this paper, we report on KIC 9693187[1], the least evolved solar-like oscillator so far, for which dynamical masses can be derived through a combination of *Gaia* DR3 astrometry and ground-based SB2 spectroscopy from the Las Cumbres Observatory Global Telescope Network (LCO, Brown et al. 2013). The star has the spectral type G1V and was identified and characterized as a solar-like oscillator by Chaplin et al. (2014) from *Kepler* photometry. The global seismic parameters ($\nu_{\rm max}$, $\Delta\nu$, Mathur et al. 2022, see Table 2) and position in the magnitude-color diagram (Godoy-Rivera et al. 2025) suggest that KIC 9693187 is on the MS or an early sub-giant (eSG).

To obtain the mass, radius and age of MS and eSG solar-like oscillators, Serenelli et al. (2017) performed a grid-modeling matching $\nu_{\rm max}$, $\Delta\nu$, the effective temperature ($T_{\rm eff}$), and the metallicity ([Fe/H] = -0.164 dex) with the properties of theoretical isochrones. For this object, Serenelli et al. (2017) report two masses for the oscillator 0.99±0.03 $M_{\odot}$ and 1.12±0.03 $M_{\odot}$. The main difference between the values is rooted in the different effective temperatures used for the scaling relations, 5790 K from parameters based on the $T_{\rm eff}$-scale of the Sloan Digitized Sky Survey, and 6214 K from APOGEE Stellar Parameters and Chemical Abundances Pipeline (ASPCAP). This difference in mass leads to distinct stellar ages (~10 vs. ~5 Gyr) and highlights the dependence of the scaling relations on spectroscopy.

Molenda-Żakowicz et al. (2013) reported this system as a double-lined spectroscopic binary (SB2) but did not provide orbital parameters. Eventually, the Gaia Collab. et al. (2023) reported this system as ASB1, in the Two-Body Orbit solutions (TBO), within the NSS. In addition to the orbital parameters ($P_{\rm orb}$=103.75±0.13 days, e=0.39±0.04), the TBO also reports the inclination angle, i of the orbital plane to be 66±2 degrees.

2. Spectroscopic analysis and dynamical masses

We monitored KIC 9693187 with NRES (Network of Robotic Echelle Spectrographs, Brown et al. 2013), mounted on the 1 m telescopes of the northern LCO nodes at McDonald Observatory (USA) and Wise Observatory (Israel). NRES is an échelle spectrograph with a resolution of $R \simeq 53{,}000$. Between April 2023 and June 2024, we have collected 22 spectra of KIC 9693187.

The NRES pipeline calculates the cross-correlation function's response profile (CCF) from the observed spectra and a synthetic spectrum as a template to compute the radial velocitis (RV). The pipeline automatically selected the most appropriate template from the Phoenix model library, based on the *Gaia* parameters of the target ($T_{\rm eff}$ = 5700 K, $\log g$ = 4 dex, [Fe/H] = 0 dex). The CCF profiles of the individual spectra, shown in Fig. 1 clearly reveal the SB2 nature of KIC 9693187.

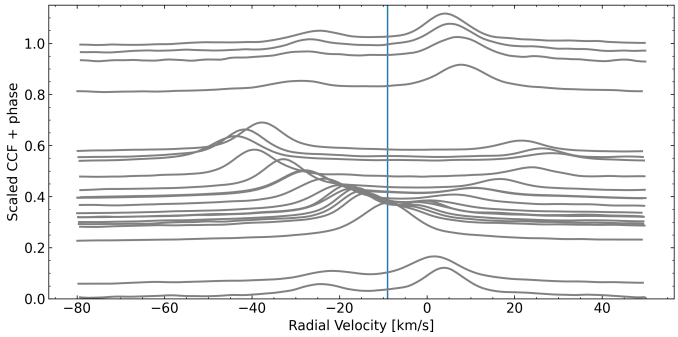

Fig. 1. CCF profiles for KIC 9693187, as a function of the orbital phase.

2.1. Spectral disentangling

To determine the RV semi-amplitudes of the primary and secondary, K_1 and K_2 respectively, we applied spectral disentangling (SPD) in Fourier space. This technique optimizes the orbital elements of a binary, including K_1 and K_2 (Simon & Sturm 1994; Hadrava 1995). We note that we refer to the more massive component as the primary, indicated with the subscript 1.

For our SPD analysis of KIC 9693187, we use the FDBinary code (Ilijic et al. 2004). We focused on a 60 nm wide region between 476.1 and 536.1 nm, including the Mg-triplet, which is well suited to determine K for both components. The disentangled spectra are depicted in Fig. A.1. Except for the orbital period, which we fix to the astrometric solution from the *Gaia* TBO, we treated all orbital parameters as free parameters. The resulting values are reported in Table 1. The uncertainties were derived from a Gaussian fit to the parameter distributions from 5000 bootstrap simulations (see Pavlovski et al. 2023).

The best solution finds K_1=26.298 ±0.058 km/s and K_2=29.394 ±0.066 km/s as the RVs semiamplitudes for the primary and secondary component. These values reveal a mass ratio of $q = M_2/M_1$ =0.8947 ±0.0028. This translates into a difference in mass of ~11%. From the disentangled spectra we get a line-depth ratio in the disentangled wavelength range (Fig. A.1) of about ~68:~32, which is a proxy for the fractional-light ratio between both components in Johnson V.

2.2. Stellar fundamental parameters

Fundamental stellar parameters were derived through a spectroscopic analysis using an updated version of the 1D/LTE code BACCHUS (Masseron et al. 2016; Hayes et al. 2022). The full analysis and derived parameters are provided in App. A.1 and Table 1. We find an effective temperature of 5738 ±84K and a sub-solar metallicity ([Fe/H]=-0.36 ±0.15dex). The significant enrichment of α elements ([α/Fe]=+0.25 ±0.05dex) indicates that the star is member of the older thick-disk population. The projected surface rotation velocity, $v \sin i$ of the primary and secondary are more than twice the current solar value and about four times faster than the expected $v \sin i$ at the MS turnoff of the Sun. Even more puzzling, no photometric signature of spot-

[1] = Gaia DR3 2107491287660520832 = 2MASS J18510009+4625209

Table 1. Orbital and fundamental parameters for KIC 9693187.

Parameter		Primary	Secondary
$P_{\rm orb}$	[d]	103.75 ±0.13 (fixed)	
e		0.3926 ±0.0016	
ω	[deg]	225.98 ±0.53	
K	[km/s]	26.298 ±0.058	29.394 ±0.066
q	$= M_2/M_1$	0.8947 ±0.0028	
T_0	MJD	60020.40 ±0.11	
$T_{\rm eff}$	[K]	5738 ±84	5150 ±150
$\log g$	[dex]	4.00 ±0.37	4.5 (fixed)
$v \sin i$	[km/s]	6.7 ±1.5	8 ±2
$\xi_{\rm micro}$	[km/s]	1.21 ±0.07	1.0 (fixed)
[Fe/H]	[dex]	-0.36 ±0.15	
[α/Fe]	[dex]	+0.25 ±0.05	
[M/H]	[dex]	+0.18 ±0.15	
L_1/L_2		2.6 ±0.1	
$M_1^{\rm dyn}$	[$M_\odot$]	0.993 ±0.046	0.889 ±0.041

Notes. The table notes are provided in Appendix A.2.

modulation is seen in the lightcurve or PSD (García et al. 2014; Santos et al. 2021, see also Fig. 2 below 1 μHz).

2.3. Dynamical masses

We calculate the dynamical masses for both components,

$$\frac{M_{1,2}}{M_\odot} = \frac{K_{2,1}\cdot(K_1+K_2)^2}{M_\odot G}\cdot\frac{P\cdot(1-e^2)^{3/2}}{2\pi\cdot\sin^3 i}\,, \tag{3}$$

using the determined orbital parameters and $K_{1,2}$ from spectroscopy (Table 1), and $P_{\rm orb}$ and inclination, i, provided by *Gaia*. We obtain $M_1^{\rm dyn}$=0.993±0.046 $M_\odot$ and $M_2^{\rm dyn}$=0.889±0.041 $M_\odot$.

3. Asteroseismology of KIC 9693187

3.1. Global seismology

From the global seismic values reported in (Mathur et al. 2022, see Table 2), and the effective temperature from our spectroscopic analysis the scaling relations (Eq. 1, 2) yield a stellar mass, $M_1^{\rm SR} = 0.98 \pm 0.18\,M_\odot$, and radius, $R_1^{\rm SR} = 1.42 \pm 0.10\,R_\odot$.

3.2. Individual-frequency seismology

We searched for the best stellar model, constrained by using individual-frequency seismology. We re-extracted the light-curve and calculated the power-spectral density (PSD, Fig. B.1) following the procedure described in App. B. Using `apollinaire` (Breton et al. 2021), we extracted 28 frequencies of the spherical degree, $\ell = 0$, 1, and 2. The extracted frequencies (see Table A.1) are depicted in the échelle diagram (Fig. 2).

The structural modeling was done with the MESA stellar evolution code package (Modules for Experiments in Stellar Astrophysics, Jermyn et al. 2023; Paxton et al. 2011, and references therein). The frequencies were calculated from each model using the GYRE code package (Townsend & Teitler 2013). The modeling setup is described in more detail in App. B.3. While the $T_{\rm eff}$, metallicity, and the seismic luminosity and $\log g$ are input parameters, the large number of individual frequencies dominates the error, leading to smaller uncertainties and robust values (Lebreton & Goupil 2014; Grossmann et al. 2025). The model that fits best the observational constraints is found with a mass of

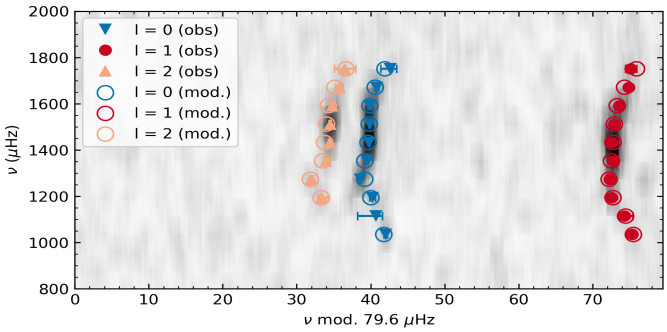

Fig. 2. Echelle diagram of the target for the observed (closed symbols) and modeled (open symbols) oscillation modes.

Table 2. Seismic parameters for the primary of KIC 9693187.

Parameter		Value
$\nu_{\rm max}$	[μHz]	1527 ±74
$\Delta\nu$	[μHz]	79.6 ±2.1
$M_1^{\rm SR}$	[$M_\odot$]	0.98 ±0.18
$R_1^{\rm SR}$	[$R_\odot$]	1.42 ±0.10
$M_1^{\rm IF}$	[$M_\odot$]	0.92 ±0.01
$R_1^{\rm IF}$	[$R_\odot$]	1.38 ±0.01
$A_1^{\rm IF}$	[Gyr]	11.20 ±0.55

Notes. The table notes are provided in Appendix B.1.

$M_1^{\rm IF}$=0.92±0.01 $M_\odot$ and radius of $R_1^{\rm IF}$=1.38±0.01 $R_\odot$. The model frequencies in the échelle diagram (Fig. 2) present a good fit.

4. Discussion & Conclusions

For the oscillating primary component, we find excellent agreement between the dynamical mass, $M_1^{\rm dyn} = 0.993 \pm 0.046\,M_\odot$, and the mass derived from asteroseismic scaling relations, $M_1^{\rm SR} = 0.98 \pm 0.18\,M_\odot$. The mass obtained from detailed seismic modeling using individual frequencies, $M_1^{\rm IF} = 0.92 \pm 0.01\,M_\odot$, agrees with the dynamical mass within 1.55σ, where σ denotes the combined uncertainty from both measurements. The best-fitting seismic model reproduces the observables well, as indicated by a reduced $\chi^2_{\rm red} = 1.53$ and the corresponding échelle diagram shown in Fig. 2. The small formal uncertainty in the IF seismic mass reflects internal modeling precision. However, results from the hare-and-hounds exercise by Cunha et al. (2021) suggest typical systematic deviations of up to 4.32% in mass, 1.33% in radius, and 11.25% in age. Accounting for such systematics, the uncertainty in the IF seismic mass would increase to approximately 0.04 $M_\odot$, leading to a difference of 1.2σ relative to the dynamical value. Therefore, the level of agreement between the dynamical and seismic masses remains robust.

The best-fit IF model yields an age of 11.20 ±0.55 Gyr for the primary component of KIC 9693187 (Table 2). This result confirms the evolved nature of the star, placing it at the main-sequence turnoff, at the point of core hydrogen exhaustion, while the secondary remains on the main sequence (Fig. 3). This evolutionary configuration is consistent with the α-enhanced chemical composition of the system. However, given the advanced age of the primary, the rapid surface rotation remains puzzling.

The uncertainty on the derived dynamical masses remains relatively large compared to the sub-percent precision that is in

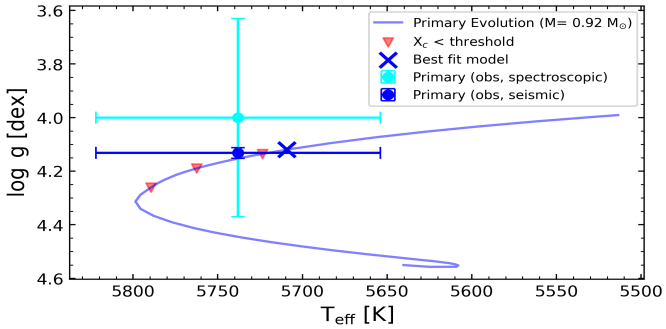

Fig. 3. Kiel diagram of the primary of KIC 9693187. The spectroscopic and seismic log g are depicted for the primary. The evolutionary track of the main sequence and the sub-giant phase is shown. The red triangles show when the fractional core-H content X_c drops below 1%, 0.01%, and 0.0001% and the blue cross gives the position of the best fit model.

principle achievable with this method (Torres et al. 2010). A major contributor is the relatively large error of ±2° on the orbital inclination, which significantly contributes to the uncertainty. Looking ahead, larger sample sizes with improved constraints on orbital inclination and the availability of epoch RV in the forthcoming *Gaia* DR4 that can be combined with ground based RV monitoring, will enable rapid progress in refining dynamical mass measurements for solar-like oscillators in binaries.

As suggested by Beck et al. (2024), the combination of *Gaia* astrometry of non-eclipsing systems with SB2 solutions from ground-based spectroscopy, or from forthcoming *Gaia* DRs, offers a promising and abundant new source of benchmark calibrators. These developments are particularly timely in light of the upcoming ESA mission PLATO (PLAnetary Transits and Oscillations of stars; Rauer et al. 2025), which will provide high-precision asteroseismic data for ten thousands of solar-like oscillators. A significant number of ASB1 systems identified in *Gaia* DR3 as astrometric binaries and potentially hosting a solar-like oscillator on the MS, SG, or red-giant phase have been selected by the authors as part of the Science Calibration and Validation PLATO Input Catalog (scvPIC, Zwintz et al. 2025). The NRES/LCO monitoring presented in this work is part of a dedicated follow-up program to build a sample of such high-value targets with SB2 signatures. This growing sample of well-calibrated benchmark stars not only enables broader validation of global asteroseismic methods, but also offers a rich ensemble of well calibrated stars to test complex aspects of stellar evolution from physics-informed models (e.g. Grossmann et al. 2025; Thomsen et al. 2025; Schimak et al. 2025). Ultimately, these efforts will support PLATO's core scientific objective of improving the precision of stellar age determinations.

Acknowledgements. The authors thank the people behind the ESA *Gaia*, NASA *Kepler* mission and the LCOT project. The authors wish to acknowledge the contribution of the IAC High-Performance Computing support team and hardware facilities to the results of this research. PGB acknowledges support by the Spanish Ministry of Science, Innovation and Universities (MCIN) with the *Ramón y Cajal* fellowship (RYC-2021-033137-I, MRR4032204). PGB, TM, DGR, DHM, JM, and IA acknowledge support from MCIN for the project*PLAtoSOnG* from its grant PID2023-146453NB-100, PI: Beck) and DHG, SM, DGR, RAG and HJD acknowledge similar support from grant PID2023-149439NB-C41. DGR acknowledges support from the Juan de la Cierva program under contract JDC2022-049054-I. DHG received support of a fellowship from *"la Caixa" Foundation* (ID 100010434, LCF/BQ/DI23/11990068). JM was supported by the Czech Science Foundation (GACR), project no. 24-10608O. DBP, RAG, and EP acknowledge the support from the GOLF and PLATO Centre National D'Études Spatiales grants. YL acknowledges support from STFC studentship ST/W507453/1 and ERC Consolidator Grant GAIA-BIFROST (Grant ID 101003096). This work was supported by the International Space Science Institute (ISSI) in Bern (project 24-629).
This article is based on observations made with the NRES spectrograph mounted on the 1 m telescopes LCOGT telescopes, one of whose nodes is located at the Observatorios de Canarias del IAC on Tenerife at Teide Observatory. This work has made use of data from the European Space Agency (ESA) mission *Gaia*, processed by the *Gaia* Data Processing and Analysis Consortium (DPAC). Funding for the DPAC has been provided by national institutions, in particular the institutions participating in the *Gaia* Multilateral Agreement. Data collected with the *Kepler* mission, obtained from the MAST data archive at the Space Telescope Science Institute (STScI) was used. STScI is operated by the Association of Universities for Research in Astronomy, Inc., under NASA contract NAS 5–26555.

References

Alexeeva, S., Ryabchikova, T., Mashonkina, L., & Hu, S. 2018, ApJ, 866, 153
Beck, P. G. 2025, A&A (under revision)
Beck, P. G., do Nascimento, Jr., J.-D., Duarte, T., et al. 2017, A&A, 602, A63
Beck, P. G., Grossmann, D. H., Steinwender, L., et al. 2024, A&A, 682, A7
Bellinger, E. P. 2020, MNRAS, 492, L50
Benbakoura, M., Gaulme, P., McKeever, J., et al. 2021, A&A, 648, A113
Borucki, W. J., Koch, D., Basri, G., et al. 2010, Science, 327, 977
Breton, S. N., García, R. A., Ballot, J., et al. 2022, A&A, 663, A118
Breton, S. N., Santos, A. R. G., Bugnet, L., et al. 2021, A&A, 647, A125
Brown, T. M., Baliber, N., Bianco, F. B., et al. 2013, PASP, 125, 1031
Brown, T. M., Gilliland, R. L., Noyes, R. W., et al. 1991, ApJ, 368, 599
Casagrande, L., Silva Aguirre, V., Schlesinger, K. J., et al. 2016, MNRAS, 455, 987
Chaplin, W. J., Basu, S., Huber, D., et al. 2014, ApJS, 210, 1
Christensen-Dalsgaard, J. 2008, Ap&SS, 316, 113
Cox, J. P. & Giuli, R. T. 1968, Principles of stellar structure
Cunha, M. S., Roxburgh, I. W., Aguirre Børsen-Koch, V., et al. 2021, MNRAS, 508, 5864
Domingo, V., Fleck, B., & Poland, A. I. 1995, Sol. Phys., 162, 1
Doyle, A. P., Davies, G. R., Smalley, B., et al. 2014, MNRAS, 444, 3592
Foreman-Mackey, D., Hogg, D. W., Lang, D., et al. 2013, PASP, 125, 306
Gaia Collab., Arenou, F., Babusiaux, C., et al. 2023, A&A, 674, A34
Gaia Collab., Prusti, T., de Bruijne, J. H. J., et al. 2016, A&A, 595, A1
Gaia Collaboration, Vallenari, A., Brown, A. G. A., et al. 2023, A&A, 674, A1
García, R. A. & Ballot, J. 2019, Living Reviews in Solar Physics, 16, 4
García, R. A., Hekker, S., Stello, D., et al. 2011, MNRAS, 414, L6
García, R. A., Mathur, S., Pires, S., et al. 2014, A&A, 568, A10
García, R. A., Mathur, S., Hookway, G. T., et al. 2025, A&A (submitted)
Gaulme, P., McKeever, J., Jackiewicz, J., et al. 2016a, ApJ, 832, 121
Gaulme, P., Rowe, J. F., Bedding, T. R., et al. 2016b, ApJ, 833, L13
Godoy-Rivera, D. & Chanamé, J. 2018, MNRAS, 479, 4440
Godoy-Rivera, D., Mathur, S., García, R. A., et al. 2025, A&A, 696, A243
González-Cuesta, L., Mathur, S., García, R. A., et al. 2023, A&A, 674, A106
Grevesse, N. & Sauval, A. J. 1998, Space Sci. Rev., 85, 161
Grossmann, D. H., Beck, P. G., Mathur, S., et al. 2025, A&A, 696, A42
Gustafsson, B. 2008, Physica Scripta Volume T, 130, 014036
Hadrava, P. 1995, AAPS, 114, 393
Hayes, C. R., Masseron, T., Sobeck, J., et al. 2022, ApJS, 262, 34
Heiter, U., Lind, K., Bergemann, M., et al. 2021, A&A, 645, A106
Hilditch, R. W. 2001, An Introduction to Close Binary Stars
Howell, S. B., Sobeck, C., Haas, M., et al. 2014, PASP, 126, 398
Huber, D., White, T. R., Metcalfe, T. S., et al. 2022, AJ, 163, 79
Iglesias, C. A. & Rogers, F. J. 1996, ApJ, 464, 943
Ilijic, S., Hensberge, H., Pavlovski, K., et al. 2004, ASPCS, 318, 111
Jermyn, A. S., Bauer, E. B., Schwab, J., et al. 2023, ApJS, 265, 15
Kallinger, T., Mosser, B., Hekker, S., et al. 2010, A&A, 522, A1
Kjeldsen, H. & Bedding, T. R. 1995, A&A, 293, 87
Lebreton, Y. & Goupil, M. J. 2014, A&A, 569, A21
Masseron, T., Johnson, J. A., Lucatello, S., et al. 2012, ApJ, 751, 14
Masseron, T., Merle, T., & Hawkins, K. 2016, BACCHUS, Astrophysics Source Code Library, record ascl:1605.004
Mathur, S., García, R. A., Breton, S., et al. 2022, A&A, 657, A31
Mathur, S., García, R. A., Huber, D., et al. 2016, ApJ, 827, 50
Mathur, S., García, R. A., Régulo, C., et al. 2010, A&A, 511, A46
Metcalfe, T. S., Chaplin, W. J., Appourchaux, T., et al. 2012, ApJL, 748, L10
Moe, M. & Di Stefano, R. 2017, ApJS, 230, 15
Molenda-Żakowicz, J., Sousa, S. G., Frasca, A., et al. 2013, MNRAS, 434, 1422
Offner, S. S. R., Moe, M., Kratter, K. M., et al. 2023, 534, 275
Osorio, Y. & Barklem, P. S. 2016, A&A, 586, A120
Pavlovski, K., Southworth, J., Tkachenko, A., et al. 2023, A&A, 671, A139
Paxton, B., Bildsten, L., Dotter, A., et al. 2011, ApJS, 192, 3
Pérez Hernández, F., García, R. A., Mathur, S., Santos, A. R. G., & Régulo, C. 2019, Frontiers in Astronomy and Space Sciences, 6, 41
Pinsonneault, M. H., Zinn, J. C., Tayar, J., et al. 2025, ApJS, 276, 69
Pires, S., Mathur, S., García, R. A., et al. 2015, A&A, 574, A18
Prša, A. 2018, Phoebe 2 - Modeling and Analysis of Eclipsing Binary Stars
Rauer, H., Aerts, C., Cabrera, J., et al. 2025, ExpAstro, 59, 26
Ricker, G. R., Winn, J. N., Vanderspek, R., et al. 2014, SPIE, 9143, 914320
Roca Cortés, T., Jiménez, A., Pallé, P. L., GOLF team, & VIRGO Team. 1999, in Magnetic Fields and Solar Processes, ed. A. Wilson & et al., Vol. 448, 135
Salaris, M., Chieffi, A., & Straniero, O. 1993, ApJ, 414, 580
Santos, A. R. G., Breton, S. N., Mathur, S., & García, R. A. 2021, ApJS, 255, 17
Schimak, L. S., Bedding, T. R., Crawford, C. L., et al. 2025, MNRAS, submitted
Serenelli, A., Johnson, J., Huber, D., et al. 2017, ApJS, 233, 23
Simon, K. P. & Sturm, E. 1994, A&A, 281, 286
Thomsen, J. S., Miglio, A., Brogaard, K., et al. 2025, A&A, 699, A152
Torres, G., Andersen, J., & Giménez, A. 2010, A&Ar, 18, 67
Townsend, R. H. D. & Teitler, S. A. 2013, MNRAS, 435, 3406
White, T. R., Benomar, O., Silva Aguirre, V., et al. 2017, A&A, 601, A82
Zinn, J. C., Stello, D., Elsworth, Y., et al. 2022, ApJ, 926, 191
Zwintz, K., Heller, R., Maxted, P., et al. 2025, ExpAstro (submitted)

Appendix A: Spectroscopic analysis

A.1. Fundamental parameters

Fundamental stellar parameters were derived through a spectroscopic analysis using an updated version of the 1D/LTE code BACCHUS (Brussels Automatic Code for Characterizing High accUracy Spectra, Masseron et al. 2016; Hayes et al. 2022), which employs MARCS model atmospheres (Gustafsson 2008) and the atomic and molecular line lists from Heiter et al. (2021). For the specific case of SB2 spectra, the code has been newly extended to compute a secondary synthetic spectrum on the fly, with fixed stellar parameters, a given radius ratio, and the appropriate radial velocity shift. This secondary spectrum is treated as a perturbation to the primary spectrum, adding continuum opacities of both components, and possibly line opacities when analyzing non-disentangled spectra. Thus, from the perspective of the code, such implementation allows to indifferently swap the analysis of each component.

Effective temperatures were determined by requiring no trend between the abundances derived from Fe I lines and their excitation potentials. Surface gravity was obtained by enforcing ionization balance between Fe I and Fe II lines. As this method requires a large number of moderately weak Fe lines, we obtained and combined three consecutive spectra with high signal-to-noise. Microturbulence velocity was simultaneously constrained by minimizing trends between Fe line abundances and their equivalent widths. The metallicity was determined as the mean abundance of the Fe I lines. However, because the secondary component of KIC 9693187 contributes significantly less to the overall flux, only the strongest lines could be observed and analyzed. Consequently, neither the microturbulence nor the surface gravity could be constrained with our procedure relying on Fe lines and they were fixed in the determination of the parameters. The entire parameter determination process was iteratively refined, alternating the primary and secondary components analysis until convergence was reached. The temperatures of the two components were also validated by checking the quality of the fit of the wing of Hα line of the disentangled spectra.

Moreover, in SB2 systems, on a first order approximation the line-depth-ratio, thus metallicity ratio, and luminosity ratio are degenerate. We stress though, that the clear orbital motion of both components supports the assumption of a common origin and homogeneous chemical composition, as expected for coeval binaries (e.g., Godoy-Rivera & Chanamé 2018; Moe & Di Stefano 2017; Offner et al. 2023). Therefore, by enforcing equal metallicities, luminosity could be constrained. On another hand, absorption line depth may also dependent on other stellar parameters such as the effective temperature. To alleviate the stellar parameters dependence, very strong and saturated lines such as the core of the Mg triplet lines represent relevant features which depth is nearly invariant with temperature, surface gravity or metallicity in cool stars spectra. We stress that the core of Mg lines are also subject to NLTE effects (Osorio & Barklem 2016; Alexeeva et al. 2018). Caution must be taken when using those lines as luminosity indicator.

Finally, with both temperature of the two component constrained and the luminosity ratio fixed, the radii ratio could be established (Masseron et al. 2012), leading to a value of 1.4±0.05.

The code also automatically adjusts a mean line-broadening value to fit the Fe line profiles. The projected rotational velocity ($v \sin i$) was then estimated by assuming that this broadening is the quadratic sum of the instrumental resolution (R = 53,000), macroturbulence (adopted from the prescription of Doyle et al. (2014) for G–K main-sequence stars), and rotational broadening. The derived fundamental parameters are reported in Table 1.

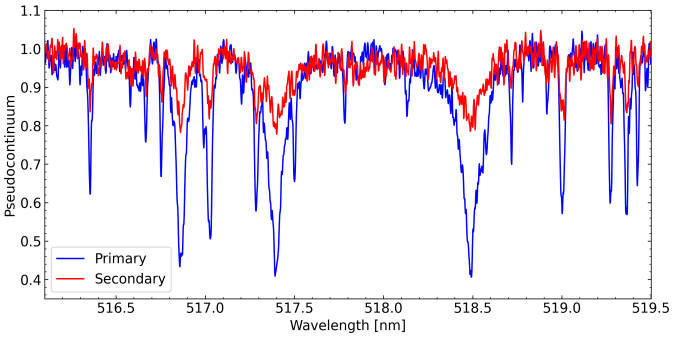

Fig. A.1. Accumulated spectra for the primary (blue) and secondary (red) of KIC 9693187 around the Mg triplet from spectral disentangling. The disentangled spectra are both normalized to the pseudocontinuum of the composite spectrum.

A.2. Notes on Table 1

The top and middle panels of Table 1 present the results from spectral disentangling and the spectroscopic analysis of the disentangled component spectra. The bottom panel reports the dynamical masses derived from the orbital parameters and the measured mass ratio.

The individual parameters and their uncertainties are described as follows:

- T_0: time of periastron passage, expressed in BJD,
- e: orbital eccentricity,
- ω [deg]: argument of periastron, indicating the angle between the ascending node and the periastron point,
- K [km/s]: radial velocity semi-amplitude of each component,
- q: mass ratio of the binary, defined as $q = M_2/M_1$, where M_1 and M_2 are the masses of the primary and secondary components, respectively,
- $T_{\rm eff}$ [K]: effective temperature of each component,
- $v \sin i$ [km/s]: projected rotational surface velocity,
- [M/H] [dex]: stellar metallicity, relative to the Sun,
- [α/Fe] [dex]: abundance of α elements,
- L [$L_\odot$]: stellar luminosity for the primary, from seismic scaling relations,
- $M_{\rm dyn}$ [$M_\odot$]: dynamical mass of each component, calculated following the formulation of Hilditch (2001), and using the orbital parameters from the disentangling solution.

Appendix B: Seismology and modeling

B.1. Notes on Table 2

The top panel of Table 2 presents seismic values for the oscillating primary of KIC 9693187, reported by Mathur et al. (2022). The middle panel reports the result for the mass ($M_{\rm SR}$) and radius ($R_{\rm SR}$) from applying the scaling relations (SR) as given in Eq. 1 and 2. Hereby, we use the solar reference values of the A2Z pipeline $\nu^{\odot}_{\rm max} = 3100\,\mu$Hz, $\Delta\nu_\odot = 135.2\,\mu$Hz, and $T_{\rm eff,\odot} = 5777$ K (Mathur et al. 2010).

The bottom panel presents the mass ($M_{\rm IF}$), radius ($R_{\rm IF}$), and age ($A_{\rm IF}$) determined for KIC 9693187 from the individual-frequency modeling (IF), described in App. B.3.

Table A.1. Frequency list for KIC 9693187.

n	ℓ	ν [μHz]	σ_ν [μHz]	Flag
12	0	1076.25	0.25	0
12	1	1109.60	0.39	0
13	0	1154.48	2.45	1
13	1	1188.09	1.15	0
13	2	1226.68	0.90	0
14	0	1233.54	0.44	0
14	1	1265.91	0.27	0
14	2	1304.83	0.29	0
15	0	1311.49	0.17	0
15	1	1345.21	0.23	0
15	2	1386.39	0.36	0
16	0	1391.91	0.18	0
16	1	1425.23	0.16	0
16	2	1466.42	0.21	0
17	0	1471.75	0.14	0
17	1	1504.59	0.12	0
17	2	1546.04	0.15	0
18	0	1551.38	0.17	0
18	1	1584.44	0.23	0
18	2	1625.84	0.37	0
19	0	1630.95	0.24	0
19	1	1664.70	0.29	0
19	2	1706.39	0.54	0
20	0	1711.43	0.28	0
20	1	1745.50	0.42	0
20	2	1786.63	1.53	0
21	0	1792.82	1.27	0
21	1	1825.31	0.85	0

Notes. n and ℓ report the radial order and the spherical degree of the extracted modes. The second and third columns provide the extracted frequency and its maximum uncertainty. The final column provides the flag for certainty, whereby 0 is a bonafide mode and 1 indicates a possible detection. Only modes with a flag=0 were used in the stellar modeling.

B.2. Peakbagging of individual modes

KIC 9693187 was observed in short cadence mode, providing one photometric measurement per minute, during two ~90-day data Quarters (Q1 and Q5). The light curves were corrected for known systematics in the *Kepler* photometry and the power-spectral density was computed following the procedures of García et al. (2011, 2014) and Pires et al. (2015). To eliminate the aliasing effects caused by the one-year gap between the quarters, we followed the common approach of shifting Q5 right after Q1.

To characterize the oscillation modes of KIC 9693187, we used the `apollinaire`[2] software package (Breton et al. 2022), which implements the `emcee` ensemble MCMC sampler (Foreman-Mackey et al. 2013). Each mode was modeled as a Lorentzian profile, with its central frequency and linewidth treated as independent parameters. A single mode height was fitted collectively for all $\ell = 0, 1$ modes of order n and for $\ell = 2$ modes of order $n-1$. Additionally, the relative height ratios between different angular degrees were included as global parameters in the fit.

For the sampling process, logarithmic forms of the amplitude and linewidth, as well as the frequency and relative mode heights, are used to ensure non-informative, uniform priors. All parameters of all modes are fitted at the same time in a global way (as first done by Roca Cortés et al. 1999).

Posterior distributions are generated for all parameters, from which the median values are adopted as best estimates. The associated uncertainties are defined by the larger deviation between the median and the 16$^{\rm th}$ or 84$^{\rm th}$ percentiles of the posterior samples. For the final error bars given in Table A.1, and following a conservative approach, the larger of the asymmetrical error obtained during the sample of the posteriors is provided.

[2] Documentation is available at `https://apollinaire.readthedocs.io/en/latest/`.

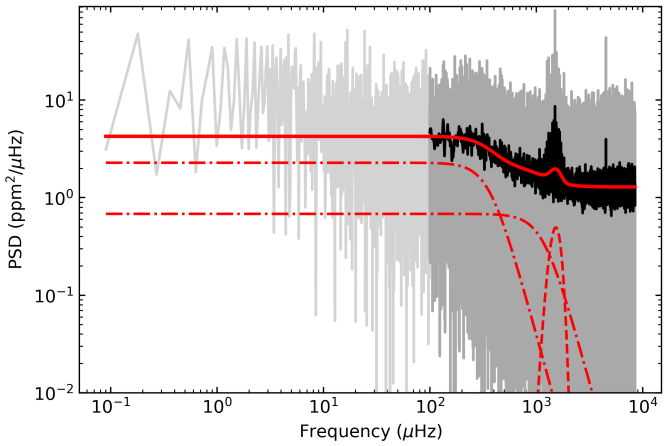

Fig. B.1. PSD of the primary of KIC 9693187. The multi-component fit to the PSD and (upper panel) and the power excess (lower panel) are shown. In the upper panel, the dash-dotted liens represent the background fits, while the dashed red line represents the gaussian fit. The solid line represents the combined fit to the PSD. The vertical dashes in the lower panel indicate the of the extracted radial (blue), dipole (dark red), and quadruple (orange). The solid red line depicts the combined solution of all extracted modes.

B.3. Individual frequency modeling with MESA

To estimate the mass, radius and age of the oscillating component, we performed a detailed seismic grid modeling of KIC 9693187. As input we used the effective temperature from the spectroscopic analysis of the LCO data. We corrected the metallicity following Salaris et al. (1993),

$$[\mathrm{M/H}] = [\mathrm{Fe/H}] + \log_{10}(0.638 \cdot 10^{[\alpha/\mathrm{Fe}]} + 0.362), \quad \text{(B.1)}$$

to account for the modified mean molecular weight in the the enrichment of α-elements. As input metallicity, we used [M/H]=-0.18 ±0.15dex. Because the secondary component contributes about 32% to the total flux in V (see Sect. 2.1), the *Gaia* luminosity would lead to overestimated values. Therefore, we used the seismic scaling relation, for the stellar luminosity

$$\frac{L}{L_\odot} = \left(\frac{\nu_{\rm max}}{\nu^\odot_{\rm max}}\right)^2 \cdot \left(\frac{\Delta\nu}{\Delta\nu_\odot}\right)^{-4} \cdot \left(\frac{T_{\rm eff}}{T_{\rm eff,\odot}}\right)^5, \quad \text{(B.2)}$$

and for the surface gravity,

$$\log g_1 = \log(g_\odot) + \log\left[\left(\frac{\nu_{\rm max,1}}{\nu_{\rm max,\odot}}\right) \cdot \sqrt{\frac{T_{\rm eff,1}}{T_{\rm eff,\odot}}}\right] \quad \text{(B.3)}$$

which yield a luminosity of $L_{1,\rm seis}$ =1.95 ±0.31 $L_\odot$ and a $\log g_{1,\rm seis}$ = 4.132±0.021 dex. The global seismic parameters (Table 2), and the individual frequencies of the modes from Table A.1 with flag 0 were used.

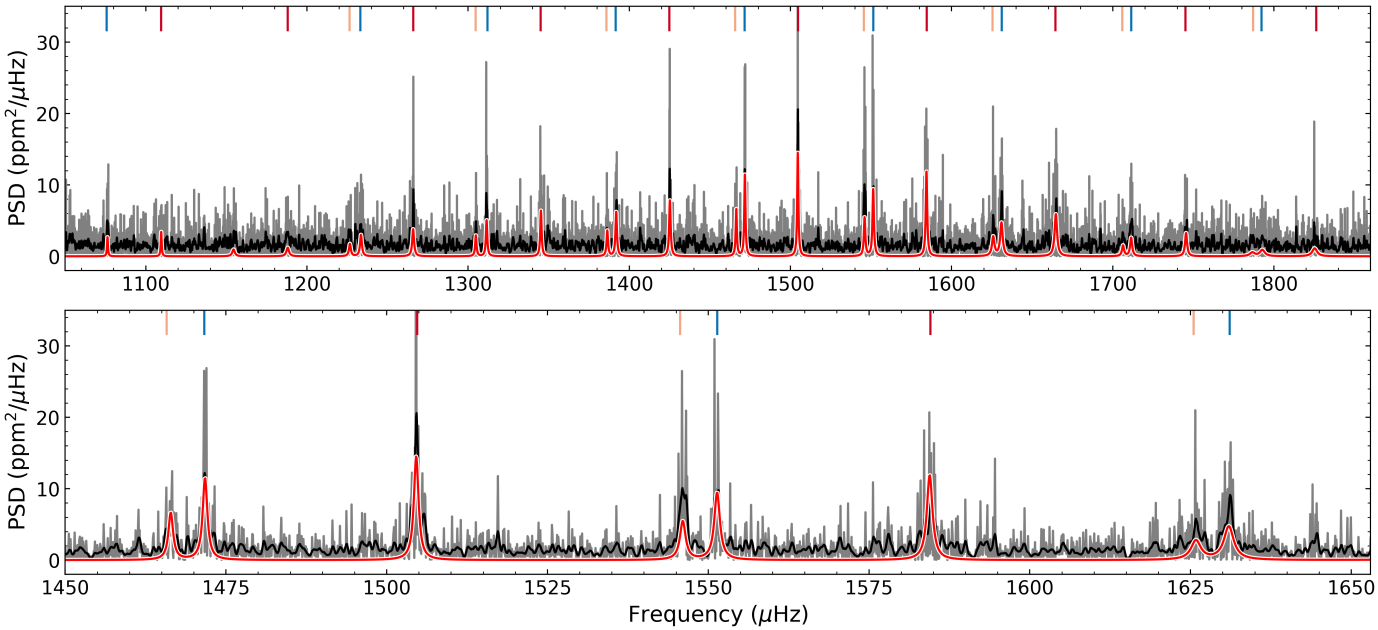

Fig. B.2. PSD of KIC 9693187 around the excess of power spectral density. The top panel shows the full power excess, with the original, and smoothed PSD in grey, and black, respectively. The lower provides a zoomed view on the two central radial orders. The red line depicts the combined model of extracted frequencies, which are represented by the vertical dashes (blue, red, and orange for ℓ=0, ℓ=1, and ℓ=2, respectively, see Table A.1.

The search for the best fitting model was performed through an iterative analysis, using the IACgrid. This collection of pre-calculated evolutionary tracks for mains-sequence stars has been computed with the MESA (Modules for Experiments in Stellar Astrophysics; version 15 140; Jermyn et al. 2023; Paxton et al. 2011) code package. The models adopt standard input physics, utilizing OPAL opacity tables (Iglesias & Rogers 1996) and the chemical composition described by (Grevesse & Sauval 1998). Stellar masses span from 0.8 to 1.5 $M_\odot$ in increments of 0.01 $M_\odot$, with initial metallicities ranging from -0.3 to +0.4 dex in steps of 0.05. The mixing-length parameter, α, varies between 1.5 and 2.2, also in steps of 0.05, following the formulation by Cox & Giuli (1968). Oscillation frequencies are computed using the adiabatic pulsation code ADIPLS (Christensen-Dalsgaard 2008), and the initial helium content is fixed at $Y_0 = 0.249$. Model fitting is performed through χ^2 minimization, where separate contributions from spectroscopic constraints, oscillation frequencies, and dynamical properties are considered. The dynamical component accounts for the characteristic timescale $(R^3/GM)^{0.5}$. Further methodological details, including the treatment of uncertainties, are provided in Pérez Hernández et al. (2019) and González-Cuesta et al. (2023).

Based on the best fit model parameters, we calculated the evolutionary track for the primary, that is shown in Fig. 3. We used the age of 12 Gyr, above 1-σ of the models age, as a stopping criterion. Fig. 3 also shows the position of KIC 9693187 according to the spectroscopic and seismic surface gravity in blue and purple, respectively. Furthermore we mark the position of the best fit model from the individual frequency modeling in the HRD. To test if KIC 9693187's primary is located before or after the turnoff from the mainsequence, we also marked the depletion of the fractional content of hydrogen in the core, whereby we mark the positions $X_c < 1\%, 0.01\%$ and 0.0001%, confirming that the star has consumed almost its core hydrogen.